

Criteria for shear banding in time-dependent flows of complex fluids

Robyn L. Moorcroft and Suzanne M. Fielding

Department of Physics, Durham University, Science Laboratories, South Road, Durham. DH1 3LE, U.K.

(Dated: January 31, 2012)

Within a highly generalised theoretical framework for the flow properties of complex fluids, we study the onset of shear banding in the three most common time-dependent experimental protocols: step stress, step strain and shear startup. By means of a linear stability analysis we derive a fluid-universal criterion for the onset of banding, separately for each protocol, that depends only on the shape of the experimentally measured time-dependent rheological response function, independent of the constitutive law and internal state variables of the particular fluid in question. Our predictions thus have the same status, in these time-dependent flows, as the widely known criterion for banding in steady state (of negatively sloping shear stress *vs.* shear rate). We support them with simulations of the rolie-poly model of polymeric fluids, the soft glassy rheology model, and a fluidity model.

PACS numbers: 61.25.he, 83.50.Ax, 62.20.F, 83.10.y, 83.60.Wc

Many complex fluids show shear banding [1], in which an initially homogeneous sample of fluid separates into layers of differing viscosity under an applied shear flow. Examples include wormlike micellar surfactants [2], polymers [3], soft glassy materials [4, 5], and (possibly) biologically active fluids [6]. At a fundamental level shear banding can be viewed as a non-equilibrium (flow-induced) phase transition, or equivalently as a hydrodynamic instability of viscoelastic origin. In practical terms it drastically alters the rheology (flow response) of these materials and thus impacts on widespread industrial applications: in plastics, foodstuffs, well-bore fluids, *etc.*

In steady state, the criterion for shear banding is (usually [7]) that the underlying homogeneous constitutive curve of shear stress *vs.* shear rate has negative slope, $d\Sigma/d\dot{\gamma} < 0$. Beyond studies in steady state, accumulating data in polymers [8–15], surfactants [16–18], soft glassy materials [19–22], and simulations [23–30] reveals that shear bands often also arise during the time-dependent process whereby a steady shear flow is established from an initial rest-state. These “transient” bands can be sufficiently long lived to represent the ultimate flow response of the material for practical purposes even if the constitutive curve is monotonic $d\Sigma/d\dot{\gamma} > 0$.

In view of these widespread observations, crucially lacking is any known criterion for the onset of banding in these time-dependent flow protocols, of the same status as given above in steady state: independent of the constitutive model and internal state variables of the particular fluid in question, and depending only on the shape of the experimentally measured rheological response function. Here we provide such criteria, separately for each of the three most common protocols: step stress, step strain and shear startup. We do so within a highly generalised framework that includes many widely used models of polymeric fluids (polymers and wormlike surfactants) and soft glassy materials (foams, dense emulsions and colloids). Our aim is thereby to develop a unified understanding of existing and future observations of time-

dependent banding; and to facilitate the design of protocols that optimally enhance or mitigate it.

Consider a sample of fluid sandwiched between parallel plates at $y = \{0, L\}$, sheared for times $t > 0$ in one of the protocols defined below. We decompose the shear stress in any fluid element into a purely Newtonian part of viscosity η , and a viscoelastic part due to the polymeric or soft glassy degrees of freedom: $\Sigma(t) = G\sigma(y, t) + \eta\dot{\gamma}(y, t)$. Translational invariance is assumed in the flow direction x and vorticity direction z . Heterogeneity is allowed in the flow gradient direction y , though force balance (neglecting inertia) demands uniform Σ . The viscoelastic shear stress $G\sigma(y, t)$, written as a modulus G times a dimensionless conformation variable σ , obeys dynamics in which loading by shear competes with intrinsic stress relaxation. In the simplest description $\partial_t \sigma = \dot{\gamma} - \frac{1}{\tau} \sigma$, though in reality this shear component $\sigma = \sigma_{xy}$ also couples to normal stress components $\sigma_{xx}, \sigma_{yy} \dots$ [31]. In models of soft glasses it also couples to (at least one) variable a characterising the sample’s fluidity [27, 32, 33]. Collecting all such variables into a vector $\mathbf{s} = (\sigma, \sigma_{xx} \dots)^T$ and defining the projection vector $\mathbf{p} = (1, 0, 0 \dots)$, we write in the most general case:

$$\Sigma(t) = G\mathbf{p} \cdot \mathbf{s}(y, t) + \eta\dot{\gamma}(y, t), \quad (1)$$

$$\partial_t \mathbf{s}(y, t) = \mathbf{Q}(\mathbf{s}, \dot{\gamma}). \quad (2)$$

For specific choices of \mathbf{s} and \mathbf{Q} , Eqns. (1, 2) encompass the predictions in shear of most commonly used rheological models. Within this general framework we will derive fluid-universal criteria for the onset of banding, separately for step stress, step strain and shear startup protocols. We support these with simulations of the rolie-poly model [34] of polymeric fluids; a fluidity model of soft glasses [27]; and the soft glassy rheology (SGR) model [27, 35]. (All these are defined in the Suppl. Mat.)

Terms of the form $D\nabla^2 \mathbf{s}$ must also be added to Eqn. 2 to prohibit flow heterogeneity at scales smaller than the fluid microstructure $l = \sqrt{D\tau}$, and to ensure unique selection of any shear banded state [36]. In any linearised

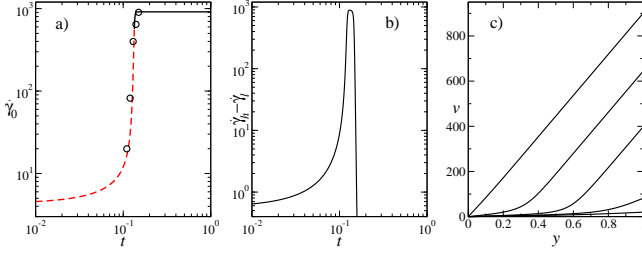


FIG. 1: a) Creep curve in the non-stretch rolie-poly model for $\beta = 0.8$, $\eta = 10^{-4}$, $\Sigma_0 = 0.7$. Dashed: linearly unstable; solid: linearly stable. b) Corresponding degree of shear banding. c) Flow profiles at times marked by circles in a) for $\epsilon_n = 0.1\delta_{n,0}$, $l = 10^{-2}$ with increasing $v(y=1)$ for increasing time t .

equation, *e.g.* (4) below, these can be neglected for the fluctuations of interest here with wavelength $\gg l$.

We use units in which the modulus $G = 1$; the rheometer gap $L = 1$; and (as defined in the Suppl. Mat.) the underlying fluid relaxation timescale $\tau_D = 1$ (rolie-poly), or $\tau_0 = 1$ (SGR and fluidity models).

Step stress protocol — Consider first an experiment in which a step stress of amplitude Σ_0 is applied to the sample at time $t = 0$. We express the response to this load as a spatially uniform “base state” of homogeneous creep, plus any (initially) small heterogeneous departure from it: $\dot{\gamma}(y, t) = \dot{\gamma}_0(t) + \sum_n \delta\dot{\gamma}_n \cos(n\pi y/L) \exp(\omega t)$, $\mathbf{s}(y, t) = \mathbf{s}_0(t) + \sum_n \delta\mathbf{s}_n \cos(n\pi y/L) \exp(\omega t)$. (Note, then, that we are studying the time-evolution of perturbations to a base state that is itself time-dependent [37].) To investigate whether at any time t the system is linearly unstable to the onset of banding, we expand Eqns. (1, 2) in powers of the heterogeneous perturbation’s amplitude and neglect terms beyond first order.

The dynamics of the homogeneous base state is specified by the zeroth order terms as follows:

$$\partial_t(\partial_t \mathbf{s}_0) = [\mathbf{M} - G\mathbf{q}\mathbf{p}/\eta] \cdot \partial_t \mathbf{s}_0 \quad (3)$$

with $\mathbf{M} = \partial_s \mathbf{Q}|_{\mathbf{s}_0, \dot{\gamma}_0}$ and $\mathbf{q} = \partial_{\dot{\gamma}} \mathbf{Q}|_{\mathbf{s}_0, \dot{\gamma}_0}$. This equation must be solved subject to the initial condition $\partial_t \mathbf{s}_0|_{t=0} = \mathbf{Q}(\mathbf{s}_0|_{t=0}, \dot{\gamma}_0(t=0) = \Sigma_0/\eta)$. The dynamics of the heterogeneous fluctuations is specified by the first order terms according to

$$\partial_t \delta \mathbf{s}_n = [\mathbf{M} - G\mathbf{q}\mathbf{p}/\eta] \cdot \delta \mathbf{s}_n. \quad (4)$$

This must be solved subject to source terms specifying the seeding of any heterogeneity, whether due to (i) sample preparation protocol, (ii) slight flow device curvature, (iii) mechanical or (iv) thermal noise. Here we consider (i), modelled as an initial condition $\delta \mathbf{s}_n(0) = \epsilon_n \mathbf{N}_n$ with each ϵ_n a small amplitude and the entries of \mathbf{N}_n chosen randomly from a flat distribution of mean 0 and width 1.

Eqns. (3, 4) reveal that the *heterogeneous* fluctuations $\delta \mathbf{s}_n$ obey, in this step stress protocol, the same dynamical equation as the time derivative $\partial_t \mathbf{s}_0$ of the *homogeneous* base state. Due to their different initial conditions,

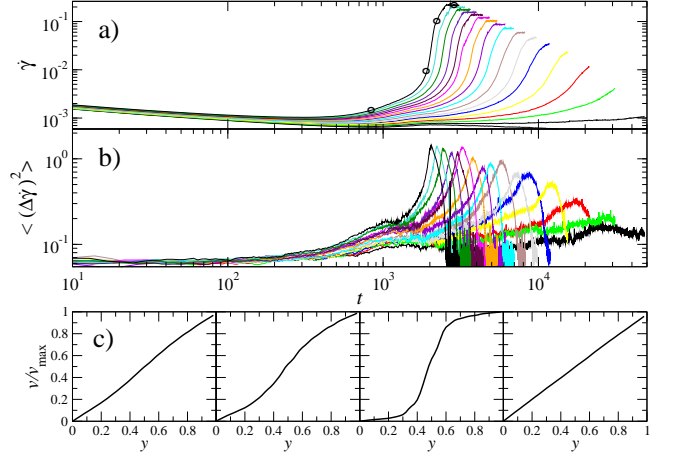


FIG. 2: a) Creep curves of the SGR model for stress values $\Sigma_0/\Sigma_y = 1.005, 1.010 \dots 1.080$ (curves upwards). b) Corresponding degree of shear banding. c) Normalised velocity profiles for the circles in a). $x = 0.3, w = 0.05, n = 50, m = 10000$. Initial sample age $t_w = 10^3 [1 + \epsilon \cos(2\pi y)]$, $\epsilon = 0.1$.

however, $\partial_t \mathbf{s}_0$ and $\delta \mathbf{s}_n$ are not guaranteed to evolve colinearly. Numerically, though, we find they always do become colinear after a very short transient. Accordingly any component of $\delta \mathbf{s}_n$ grows whenever its counterpart in \mathbf{s}_0 obeys $\partial_t^2 \mathbf{s}_0 / \partial_t \mathbf{s}_0 > 0$. Combined with the linearity of (1) this shows that banding must develop whenever the underlying homogeneous creep function $\dot{\gamma}_0(t)$ obeys $\partial_t^2 \dot{\gamma}_0 / \partial_t \dot{\gamma}_0 > 0$. This important result, valid for *any* model of the highly general form (1, 2), is consistent with numerous recent experiments in polymeric fluids [9–12, 16–18, 38] and soft glassy materials [21, 22].

We support our prediction with numerical results for the rolie-poly model [34] of polymeric fluids in Fig. 1, with parameters for which the constitutive curve $\Sigma(\dot{\gamma})$ is monotonic and the steady state unbanded. A homogeneous creep function $\dot{\gamma}_0(t)$ is shown in Fig. 1a with the regime of linear instability to the onset of banding, $\partial_t^2 \dot{\gamma}_0 / \partial_t \dot{\gamma}_0 > 0$, dashed. The corresponding degree of banding as measured in a full nonlinear simulation (Fig. 1b) is consistent with this prediction; and snapshot velocity profiles confirm obvious banding as the system starts flowing under the applied load (Fig. 1c).

We also simulated the spatially aware soft glassy rheology model [27, 35] in its glass phase, for which the steady state constitutive curve shows a yield stress Σ_y with monotonic increase beyond: $\Sigma = \Sigma_y + \alpha \dot{\gamma}^m$ with $m > 0$. For an applied stress just above Σ_y we see an early time regime of slow creep in which the shear rate progressively decreases (Fig. 2a). This then gives way to a steady flowing state via a regime of upward slope $\partial_t \dot{\gamma} > 0$ and curvature $\partial_t^2 \dot{\gamma} > 0$ in which banding arises (Fig. 2b,c), consistent with our prediction above. Homogeneous flow is recovered in steady state, though for stress values only marginally above yield the recovery time is likely to be unattainable experimentally: band-

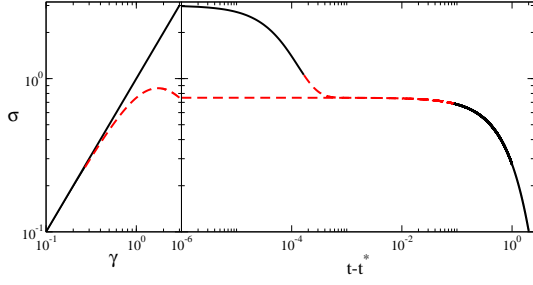


FIG. 3: Left: stress *vs.* strain for a fast ramp in the rolie-poly model. $\beta = 0.0$, $\tau_R = 10^{-4}$, $\eta = 10^{-5}$. Right: relaxation post-ramp; unstable region dashed. Upper curve: appreciable chain stretch, $\tau_R \dot{\gamma} \rightarrow \infty$. Lower: negligible stretch, $\tau_R \dot{\gamma} = 0.1$.

ing will then represent the material's ultimate observable flow response in practice.

Step strain protocol — Next we consider a rapid shear strain ramp $\gamma_0 = \dot{\gamma}_0 t$ applied for times $0 < t < t^*$, after which the strain is held constant at $\gamma_0^* = \dot{\gamma}_0 t^*$. The limit $\dot{\gamma}_0 \rightarrow \infty$ at fixed γ_0^* gives a true step. As above we analyze the response to this deformation by first (artificially) restricting the flow to remain homogeneous, then performing a linear stability analysis for the dynamics of small shear banding fluctuations about this base state.

Assuming decomposition of the viscoelastic dynamics (2) into additive loading and relaxation parts, $\dot{\gamma} \mathbf{S}$ and \mathbf{R}/τ , the base state obeys during the ramp

$$\partial_{\gamma_0} \mathbf{s}_0 = \mathbf{S}(\mathbf{s}_0) - \frac{1}{\gamma_0 \tau} \mathbf{R}(\mathbf{s}_0) \approx \mathbf{S}(\mathbf{s}_0), \quad (5)$$

dominated by loading for $\dot{\gamma}_0 \tau \gg 1$. Post-ramp it relaxes back to equilibrium according to $\partial_t \mathbf{s}_0 = -\frac{1}{\tau} \mathbf{R}(\mathbf{s}_0)$.

To investigate whether this relaxation can indeed occur in a purely homogeneous way, or whether the sample instead transiently shear bands during it (assuming t^* so short that no banding arose during the ramp itself), we write $\dot{\gamma}(y, t) = \sum_n \delta \dot{\gamma}_n \cos(n\pi y/L) \exp(\omega t)$, $\mathbf{s}(y, t) = \mathbf{s}_0(t) + \sum_n \delta \mathbf{s}_n \cos(n\pi y/L) \exp(\omega t)$ and expand to linear order to find that the heterogeneous fluctuations evolve post-ramp according to

$$\partial_t \delta \mathbf{s}_n = \left[-\frac{\mathbf{G}}{\eta} \mathbf{S}(\mathbf{s}_0) \mathbf{p} - \frac{1}{\tau} \partial_{\mathbf{s}} \mathbf{R}|_{\mathbf{s}_0} \right] \cdot \delta \mathbf{s}_n \approx -\frac{\mathbf{G}}{\eta} \mathbf{S}(\mathbf{s}_0) \mathbf{p} \cdot \delta \mathbf{s}_n \quad (6)$$

for small solvent viscosity $\eta \ll G\tau$.

Denoting by \mathbf{s}_0^* the system's state *instantaneously as the ramp ends*, we see from (5) that \mathbf{s}_0^* relates to the evolution of the base state just before the ramp ended via $\partial_{\gamma} \mathbf{s}_0|_{t=t^*-} = \mathbf{S}(\mathbf{s}_0^*)$. Because \mathbf{s}_0 is continuous at t^* , \mathbf{s}_0^* also relates (by 6) to the dynamics of the fluctuations immediately post-ramp via $\partial_t \delta \mathbf{s}_n|_{t=t^*+} = -\frac{\mathbf{G}}{\eta} \mathbf{S}(\mathbf{s}_0^*) \mathbf{p} \cdot \delta \mathbf{s}_n$. Combining these, taking the first component, and appealing to the linearity of force balance, we find

$$\partial_t \delta \dot{\gamma}_n|_{t=t^*+} = -\frac{1}{\eta} \frac{\partial \Sigma_0}{\partial \gamma}|_{t=t^*-} \delta \dot{\gamma}_n. \quad (7)$$

This result tells us that, as the system commences its relaxation back to equilibrium, it is unstable to banding

if the stress had been decreasing with strain just prior to the ramp ending. The prediction applies for any rheological model with additive loading and relaxation dynamics, and is consistent with early intuition [39].

Numerical results for the rolie-poly model (Fig. 3) support this. As discussed in the Suppl. Mat., this model has two intrinsic relaxation times: that on which a polymer chain escapes its tube of entanglements, τ_D , and that on which chain stretch relaxes, $\tau_R \ll \tau_D$. The lower curve in (3) is for a ramp rate $\dot{\gamma} \tau_D \gg 1$, $\dot{\gamma} \tau_R \ll 1$. This corresponds to the $\dot{\gamma} \rightarrow \infty$ limit of Eqn. 18 with its nonlinear loading terms: during the ramp the material behaves as a nonlinear elastic solid with a maximum of stress *vs.* strain. If the total applied strain γ^* exceeds the location of this maximum, the system is left unstable to banding immediately post-ramp. The upper curve in (3) is for a much faster ramp $\dot{\gamma} \tau_R \gg 1$. This corresponds to the $\dot{\gamma} \rightarrow \infty$ limit of Eqns. 16, which have linear loading terms. Here the material behaves as a linear elastic solid during the ramp and is stable immediately after it.

The upper curve reveals further polymer physics. Relaxation of chain stretch on the short timescale τ_R post-ramp restores a state as if no stretch had arisen in the first place: the upper curve rejoins the lower, both are unstable to banding and only finally decay on the timescale τ_D . These results are consistent with experiments [13–15, 40] and numerics [24, 26] showing that banding can either occur straight after a step strain, or following an induction period. In extensional equivalent, it might also underlie the physics of delayed necking instability [41, 42].

The fluidity and soft glassy rheology models have linearly increasing stress during a fast ramp so are predicted by Eqn. (7) to be stable against banding after it.

Shear startup — We turn finally to a shear startup experiment in which a constant strain rate $\dot{\gamma}_0$ is applied for all times $t > 0$, giving strain $\gamma_0 = \dot{\gamma}_0 t$. As always we study a base state given by the homogeneous solution $\{\dot{\gamma}_0, \mathbf{s}_0(t)\}$ of Eqns. (1, 2) in this protocol, and the dynamics of small banding fluctuations about it.

Consider first a startup run in which the sample is artificially constrained to remain homogeneous until it attains steady state $t \rightarrow \infty$. In this limit (with the constraint now removed) the criterion for instability is known to be simply $\partial_{\dot{\gamma}_0} \Sigma_0 < 0$. To generalise this to any *finite* time during startup we start by taking $\partial_{\dot{\gamma}_0} \Sigma_0|_{\dot{\gamma}_0} [(\cdot)/\dot{\gamma}_0]$, where (\cdot) denotes Eqn. 2, to find that the base state obeys

$$\partial_{\dot{\gamma}_0} \Sigma_0|_{\dot{\gamma}_0} = \mathbf{p} \cdot \mathbf{M}^{-1} \cdot [\partial_{\dot{\gamma}_0} \mathbf{s}_0|_{\dot{\gamma}_0} + \dot{\gamma}_0 \partial_{\dot{\gamma}_0} \partial_{\dot{\gamma}_0} \mathbf{s}_0 - \mathbf{q}], \quad (8)$$

with \mathbf{M}, \mathbf{q} defined as above. Heterogeneous fluctuations about this base state obey Eqn. 4, the largest eigenvalue of which crosses zero when $|\mathbf{p} \cdot \mathbf{G} \mathbf{p} + \mathbf{M}| = 0$. Combined with (8) this gives, after some manipulation, the

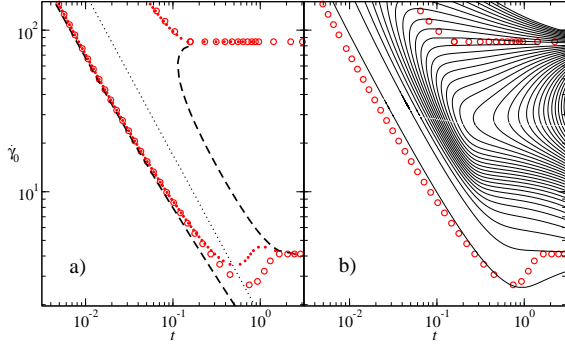


FIG. 4: Rolie-poly model with a non-monotonic constitutive curve ($\beta = 0.4, \tau_R = 0.0, \eta = 10^{-4}$). Any horizontal slice across this plane corresponds to a single shear startup run. a) Large circles: full onset criterion (9). Right dashed line: viscous criterion (10). Left dashed: elastic criterion (12). Dotted: stress overshoot $\partial_{\dot{\gamma}_0} \Sigma_0 = 0$. Small circles: elastic plus viscous terms (12)+(10). b) Circles as in a), and contour lines of equal $\delta \dot{\gamma}_n = \dot{\gamma}_0 10^M$ for integer M , from integrating Eqn. 4 with initial perturbation $\epsilon_n = 10^{-2}$. First contour: $M = -2$.

condition for banding instability during startup as

$$|\mathbf{M}| \{ \partial_{\dot{\gamma}_0} \Sigma_0|_{\dot{\gamma}_0} - \mathbf{p} \cdot \mathbf{M}^{-1} \cdot [\partial_{\dot{\gamma}_0} \mathbf{s}|_{\dot{\gamma}_0} + \dot{\gamma}_0 \partial_{\dot{\gamma}_0} \partial_{\dot{\gamma}_0} \mathbf{s}] \} < 0. \quad (9)$$

Note this contains both “viscous” derivatives with respect to strain rate $\partial_{\dot{\gamma}_0}$ (as in the steady state criterion) and now also “elastic” ones $\partial_{\dot{\gamma}_0}$ with respect to strain.

To explore the physical meaning of this result we consider now a whole series of startup runs: each at a different shear rate $\dot{\gamma}_0$, and with the evolution of the base state \mathbf{s}_0 monitored as a function of strain γ_0 (or equivalently time t) in each. Two limiting cases are instructive.

First is the steady state limit $t \rightarrow \infty$ of any individual run. Here the accumulated strain γ_0 becomes irrelevant and (9) reduces to the condition for steady state bands:

$$|\mathbf{M}| \partial_{\dot{\gamma}_0} \Sigma_0|_{\dot{\gamma}_0} < 0, \quad (10)$$

with just the viscous derivative $\partial_{\dot{\gamma}_0}$. (Note that $|\mathbf{M}| > 0$.)

The second limit concerns startup runs performed at very high rate $\dot{\gamma}_0 \rightarrow \infty$. If the stress startup curve attains a unique limiting function $\Sigma(\gamma_0)$ independent of $\dot{\gamma}_0$ in this regime (and likewise for all other components of \mathbf{s}), the material effectively then acts as a nonlinear elastic solid. Only elastic derivatives $\partial_{\dot{\gamma}_0}$ then act in (9) to give:

$$-|\mathbf{M}| \mathbf{p} \cdot \mathbf{M}^{-1} \cdot \partial_{\dot{\gamma}_0} \mathbf{s}|_{\dot{\gamma}_0} < 0, \quad (11)$$

$$-\text{tr} \mathbf{M} \partial_{\dot{\gamma}_0} \Sigma_0|_{\dot{\gamma}_0} + \dot{\gamma}_0 \partial_{\dot{\gamma}_0}^2 \Sigma_0|_{\dot{\gamma}_0} < 0, \quad (2D) \quad (12)$$

in which $\text{tr} \mathbf{M} < 0$. Here (12) specialises (11) to the case of just two degrees of freedom in \mathbf{s} as relevant, *e.g.*, to the non-stretch rolie-poly model for which $\mathbf{s} = (\sigma, \sigma_{yy})^T$.

These predictions are illustrated in Fig. 4 by numerical results for the non-stretch rolie-poly model with parameters for which the constitutive curve is non-monotonic and the steady state banded. Any horizontal slice across

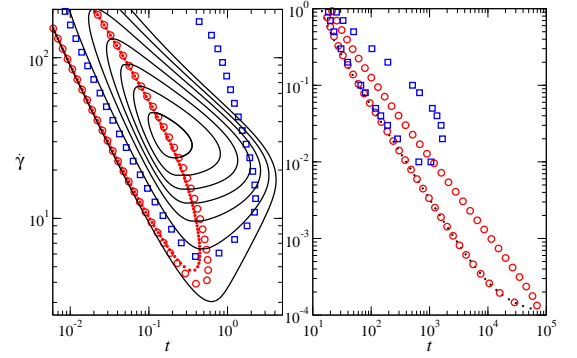


FIG. 5: Shear startup in a) rolie-poly model with a monotonic constitutive curve. $\beta = 1.0, \tau_R = 0.0, \eta = 10^{-4}$. Large circles: full onset criterion (9). Small circles: elastic plus viscous terms (12)+(10). Solid lines: contours of $\delta \dot{\gamma}_n = \dot{\gamma}_0 10^M$, from integrating Eqn. 4 with initial perturbation $\epsilon_n = 10^{-2}$. First contour: $M = -2$. b) Fluidity model for $\eta = 0.05$, initial age $t_w = 10^4$. Circles: onset criterion (9). Dashed line: $\partial_{\dot{\gamma}_0} \Sigma_0 = 0$. ϵ_n as for a) (but with perturbation added to σ only). In a) and b) squares delimit region of shear banding, $(\dot{\gamma}_h - \dot{\gamma}_l)/\dot{\gamma} > 0.05$, in *nonlinear* simulation with $l = 10^{-2}$.

this $(\dot{\gamma}_0, t)$ plane corresponds to a single startup run. “Elastic” instability (12) is apparent along any such slice at high strain rate. The first term of (12), taken alone, predicts onset of banding at the overshoot in the startup curve $\Sigma_0(\gamma_0)$; the second adds a correction to cause onset just *before* overshoot, as seen numerically. Steady state “viscous” instability (10) is seen at the far right $t \rightarrow \infty$. Between these limits the two instabilities combine and in principle one needs the full criterion (9), of which the cross terms $\partial_{\dot{\gamma}_0} \partial_{\dot{\gamma}_0}$ would be hard to measure experimentally. Pleasingly, however, simply combining criteria (10) and (12) (*i.e.*, setting the sum of their LHS’s negative) without the cross terms of (9) captures onset in most regimes, except for a small region at the lowest $\dot{\gamma}_0$. For a monotonic flow curve (Fig. 5a), steady state instability is absent but a diagonal patch of transient elastic-like instability remains.

These results are consistent with experiments [8, 10, 16, 18] and numerics [23, 24, 26, 30] for polymeric systems showing transient bands after stress overshoot, which may or may not persist to steady state depending on the slope of the ultimate flow curve.

The SGR and fluidity models do not attain a limiting startup curve $\Sigma_0(\gamma_0)$ but retain dependence on $\dot{\gamma}_0$ even as $\dot{\gamma}_0 \rightarrow \infty$. Separation into pure viscous and elastic instabilities is then not possible, though the steady state condition for banding $\partial_{\dot{\gamma}_0} \Sigma_0 < 0$ remains. Analytics for the fluidity model (which has $\partial_{\dot{\gamma}_0} \Sigma_0 > 0$ and no steady state banding) nonetheless predict a startup instability onset immediately beyond stress overshoot $\partial_{\dot{\gamma}_0} \Sigma_0 < 0$, consistent with experiment [19, 20]. Numerics further show the bands to be very long lived at low $\dot{\gamma}_0$, Fig. 5b [44]. The SGR [27] and STZ [25, 28] models (not shown) likewise

show long-lived bands onset at overshoot. It remains unclear whether this onset criterion $\partial_{\dot{\gamma}_0} \Sigma_0 < 0$ holds in *any* model (such as these) for which the stress depends strongly on strain but only logarithmically on strain rate.

Conclusion – We have given fluid-universal criteria for shear banding in time-dependent flows of complex fluids. In a step stress protocol, banding is predicted in any regime where the shear rate of the underlying creep response obeys $\partial_t^2 \dot{\gamma}_0 / \partial_t \dot{\gamma}_0 > 0$. For a fast strain ramp (“step strain”) protocol, banding instability is predicted immediately post-ramp if the stress had been decreasing with strain just prior to ending the ramp. In shear startup we predict separate “elastic” and “viscous” instabilities, and a “mixed” region between these, for a broad class of fluids that attain a limiting nonlinear stress startup curve $\Sigma(\dot{\gamma}_0)$ in fast flows $\dot{\gamma}_0 \rightarrow \infty$. In contrast the startup curve of soft glassy models retains dependence on $\dot{\gamma}_0$ even as $\dot{\gamma}_0 \rightarrow \infty$ and these fluids show a startup instability that is neither purely elastic nor viscous, onset just after stress overshoot. We hope these predictions will help unify our understanding of widespread data concerning shear banding in time-dependent flows, and stimulate further experiments to test the picture suggested here.

The authors thank Stephen Agimelen, Mike Cates, Lisa Manning, Elliot Marsden, Peter Olmsted, Lewis Smeeton and Peter Sollich for interesting discussions; and the UK’s EPSRC (EP/E5336X/1) for funding.

-
- [1] P. D. Olmsted, *Rheo. Acta* **47**, 283 (2008); S. Manneville, *ibid* **47**, 301 (2008).
 - [2] S. Lerouge and J.-F. Berret, *Adv. Polym. Sci.*, Berlin and Heidelberg (2009) Springer; M. E. Cates and S. M. Fielding, *Adv. Phys.* **55**, 799 (2006).
 - [3] P. Tapadia and S.-Q. Wang, *Phys. Rev. Lett.* **96**, 016001 (2006).
 - [4] G. Ovarlez, S. Rodts, X. Chateau, and P. Coussot, *Rheol. Acta* **48**, 831 (2009).
 - [5] P. Coussot, Q. Nguyen, H. Huynh, and D. Bonn, *J. Rheol.* **46**, 573 (2002).
 - [6] M. Cates, S. Fielding, D. Marenduzzo, E. Orlandini, and J. Yeomans, *Phys. Rev. Lett.* **101**, 068102 (2008).
 - [7] This applies for single component fluids (or multicomponent ones without strong flow-concentration coupling) in the absence of strong memory effects.
 - [8] S. Ravindranath, S.-Q. Wang, M. Olechnowicz, and R. P. Quirk, *Macromol.* **41**, 2663 (2008).
 - [9] Y. T. Hu, L. Wilen, A. Philips, and A. Lips, *J. Rheol.* **51**, 275 (2007).
 - [10] P. E. Boukany and S.-Q. Wang, *J. Rheol.* **53**, 73 (2009).
 - [11] P. Tapadia and S.-Q. Wang, *Phys. Rev. Lett.* **91**, 198301 (2003).
 - [12] S. Ravindranath and S.-Q. Wang, *J. Rheol.* **52**, 957 (2008).
 - [13] P. E. Boukany, S.-Q. Wang, and X. Wang, *Macromol.* **42**, 6261 (2009).
 - [14] S.-Q. Wang, S. Ravindranath, P. Boukany, M. Olechnowicz, R. P. Quirk, A. Halasa, and J. Mays, *Phys. Rev. Lett.* **97**, 187801 (2006).
 - [15] P. E. Boukany and S.-Q. Wang, *Macromol.* **42**, 2222 (2009).
 - [16] Y. T. Hu, C. Palla, and A. Lips, *J. Rheol.* **52**, 379 (2008).
 - [17] P. E. Boukany and S.-Q. Wang, *Macromol.* **41**, 1455 (2008).
 - [18] Y. T. Hu and A. Lips, *J. Rheol.* **49**, 1001, (2005).
 - [19] T. Divoux, C. Barentin, and S. Manneville, *Soft Matter* **7**, 9335 (2011).
 - [20] T. Divoux, D. Tamarii, C. Barentin, and S. Manneville, *Phys. Rev. Lett.* **104**, 208301 (2010).
 - [21] T. Divoux, C. Barentin, and S. Manneville, *Soft Matter* **7**, 8409 (2011).
 - [22] T. Gibaud, D. Frelat, and S. Manneville, *Soft Matter* **6**, 3482 (2010).
 - [23] J. M. Adams, S. M. Fielding, and P. D. Olmsted, *J. Rheol.* **55**, 1007 (2011).
 - [24] J. M. Adams and P. D. Olmsted, *Phys. Rev. Lett.* **102**, 067801 (2009).
 - [25] M. L. Manning, J. S. Langer, and J. M. Carlson, *Phys. Rev. E* **76**, 056106 (2007).
 - [26] L. Zhou, P. A. Vazquez, L. P. Cook, and G. H. McKinley, *J. Rheol.* **52**, 591 (2008).
 - [27] R. L. Moorcroft, M. E. Cates, and S. M. Fielding, *Phys. Rev. Lett.* **106**, 055502 (2011).
 - [28] M. L. Manning, E. G. Daub, J. S. Langer, and J. M. Carlson, *Phys. Rev. E* **79**, 016110 (2009).
 - [29] E. A. Jagla, *J. Stat. Mech.*, P12025 (2010).
 - [30] J. Cao and A. E. Likhtman, *Phys. Rev. Lett.* **108**, 028302 (2012).
 - [31] R. G. Larson, *The Structure and Rheology of Complex Fluids* (Oxford University Press, New York, 1999).

- [32] G. Picard, A. Ajdari, L. Bocquet, and F. Lequeux, Phys. Rev. E **66**, 051501 (2002).
 [33] P. Coussot, Q. D. Nguyen, H. T. Huynh, and D. Bonn, Phys. Rev. Lett. **88**, 175501 (2002).
 [34] A. Likhtman and R. Graham, J. Non-Newt. Fl. Mech. **114**, 1 (2003).
 [35] P. Sollich, F. Lequeux, P. Hébraud, and M. E. Cates, Phys. Rev. Lett. **78**, 2020 (1997).
 [36] C.-Y. D. Lu, P. D. Olmsted, and R. C. Ball, Phys. Rev. Lett. **84**, 642 (2000).
 [37] S. M. Fielding and P. D. Olmsted, Phys. Rev. Lett. **90**, 224501 (2003).
 [38] Y. T. Hu, J. Rheol. **54**, 1307 (2010).
 [39] G. Marrucci and N. Grizzuti, J. Rheol. **27**, 433 (1983).
 [40] Y. Fang, G. Wang, N. Tian, X. Wang, X. Zhu, P. Lin, G. Ma, and L. Li, J. Rheol. **55**, 939 (2011).
 [41] A. Lyhne, H. K. Rasmussen, and O. Hassager, Phys. Rev. Lett. **102**, 138301 (2009).
 [42] Y. Wang, P. Boukany, S.-Q. Wang, and X. Wang, Phys. Rev. Lett. **99**, 237801 (2007).
 [43] S. M. Fielding, M. E. Cates and P. Sollich, Soft Matter **5**, 2378 (2009).
 [44] The discrepancy between the linear and nonlinear results at low shear rates arises from our neglect of diffusive terms in the linear calculation, which do matter at very long times.
 [45] S. M. Fielding, unpublished.

SUPPLEMENTARY MATERIAL

Here we detail the governing equations of the models for which numerical results are presented in the main text. In each case we adopt the continuity equation for incompressible flow:

$$\nabla \cdot \mathbf{u} = 0, \quad (13)$$

in which \mathbf{u} is the fluid velocity field. We also impose force balance at zero Reynolds number:

$$\nabla \cdot (G\boldsymbol{\sigma} + 2\eta\mathbf{D}) = 0, \quad (14)$$

in which $\mathbf{D} = \frac{1}{2}(\mathbf{K} + \mathbf{K}^T)$ with $\mathbf{K} = \nabla\mathbf{u}$. Eqn. 14 corresponds to Eqn. 2 in the main text, with incompressibility (Eqn. 13) automatically ensured for any flow of the form considered throughout this work, with spatial variations only in the flow gradient direction. The viscoelastic dynamics of $\boldsymbol{\sigma}$ are specified for each model separately as follows.

Rolie-poly model of polymeric fluids

The rolie-poly model [34] of polymers and wormlike micellar surfactants has

$$\frac{d\boldsymbol{\sigma}}{dt} = \mathbf{K} \cdot \boldsymbol{\sigma} + \boldsymbol{\sigma} \cdot \mathbf{K}^T - \frac{1}{\tau_D}(\boldsymbol{\sigma} - \mathbf{I}) - \frac{2}{\tau_R}(1 - A) [\boldsymbol{\sigma} + \beta A^{-2\delta}(\boldsymbol{\sigma} - \mathbf{I})]. \quad (15)$$

in which $A = \sqrt{3/T}$ for molecular trace $T = \sigma_{xx} + \sigma_{yy} + \sigma_{zz}$. In this equation τ_D is the characteristic time for a polymer chain to reptate out of its tube of entanglements and τ_R is the timescale on which chain stretch relaxes. Following [34] we set $\delta = -1/2$ throughout. In planar shear flow for which $\mathbf{u} = \dot{\gamma}y\hat{\mathbf{x}}$, Eqn. (15) has componentwise dynamics

$$\begin{aligned} \partial_t \sigma &= \dot{\gamma} \sigma_{yy} - \frac{1}{\tau_D} \sigma - \frac{2}{\tau_R}(1 - A)(1 + \beta A)\sigma, \\ \partial_t \sigma_{yy} &= -\frac{1}{\tau_D}(\sigma_{yy} - 1) - \frac{2}{\tau_R}(1 - A) [\sigma_{yy} + \beta A(\sigma_{yy} - 1)], \\ \partial_t T &= 2\dot{\gamma}\sigma - \frac{1}{\tau_D}(T - 3) - \frac{2}{\tau_R}(1 - A) [T + \beta A(T - 3)]. \end{aligned} \quad (16)$$

These equations fit the generalised framework in the main text with a three dimensional $\mathbf{s} = (\sigma, \sigma_{yy}, T)^T$.

In the limit of fast chain stretch relaxation $\tau_R \rightarrow 0$ Eqn. (15) reduces to

$$\frac{d\boldsymbol{\sigma}}{dt} = \mathbf{K} \cdot \boldsymbol{\sigma} + \boldsymbol{\sigma} \cdot \mathbf{K}^T - \frac{1}{\tau_D}(\boldsymbol{\sigma} - \mathbf{I}) - \frac{2}{3}\text{tr}(\mathbf{K} \cdot \boldsymbol{\sigma}) [\boldsymbol{\sigma} + \beta(\boldsymbol{\sigma} - \mathbf{I})], \quad (17)$$

with componentwise dynamics

$$\begin{aligned} \partial_t \sigma &= \dot{\gamma} \left[\sigma_{yy} - \frac{2}{3}(1 + \beta)\sigma^2 \right] - \frac{1}{\tau_D} \sigma, \\ \partial_t \sigma_{yy} &= \frac{2}{3}\dot{\gamma} [\beta\sigma - (1 + \beta)\sigma\sigma_{yy}] - \frac{1}{\tau_D}(\sigma_{yy} - 1), \end{aligned} \quad (18)$$

and $T = 3$. These fit the framework in the main text with a two dimensional $\mathbf{s} = (\sigma, \sigma_{yy})^T$.

As noted in the main text, a diffusive term of the form $D\nabla^2\boldsymbol{\sigma}$ must be added to Eqn. 15 in any spatially resolved simulation of the shear banded profiles.

A fluidity model of soft glasses

A simple fluidity model of soft glassy rheology has

$$\frac{d\boldsymbol{\sigma}}{dt} = \mathbf{K} \cdot \boldsymbol{\sigma} + \boldsymbol{\sigma} \cdot \mathbf{K}^T - \frac{1}{\tau}(\boldsymbol{\sigma} - \mathbf{I}), \quad (19)$$

with the stress relaxation time τ ascribed its own dynamical evolution according to

$$\frac{d\tau}{dt} = 1 - \frac{\tau}{\tau_0 + 1/\sqrt{2\text{tr}\mathbf{D}\cdot\mathbf{D}}}. \quad (20)$$

In a planar shear flow $\mathbf{u} = \dot{\gamma}y\hat{\mathbf{x}}$ this model has componentwise dynamics

$$\begin{aligned} \partial_t \sigma &= \dot{\gamma} - \frac{1}{\tau} \sigma, \\ \partial_t \tau &= 1 - \frac{\tau}{\tau_0 + 1/|\dot{\gamma}|}. \end{aligned} \quad (21)$$

Transforming $\tau \rightarrow a = 1/\tau$ this fits the framework in the main text for $\mathbf{s} = (\sigma, a)$ with a fluidity variable a . Spatially diffusive terms must again be included in any simulation of the shear banded profiles. In this case model we add these only to the fluidity variable τ following [27].

The soft glassy rheology model

The soft glassy rheology model in its original (homogeneous) form [35] considers an ensemble of elements undergoing activated hopping over local energy barriers E , governed by a noise temperature x . Each element is assigned a local strain l which, between hops, obeys $\dot{l} = \dot{\gamma}$ where $\dot{\gamma}$ is the externally applied shear rate. The characteristic hop time of an element is

$$\tau = \tau_0 \exp\left(\frac{E - \frac{1}{2}kl^2}{x}\right). \quad (22)$$

After any hop, an element resets its local strain $l \rightarrow 0$ and chooses a new yield energy E at random from a distribution $\rho(E) = \exp(-E)$. The evolution of the ensemble's distribution $P(E, l, t)$ of yield energies and local strains [35] can be cast exactly in terms of the corresponding dynamics of infinitely many stress- and fluidity-like moments [45].

$$P_{m,n} = \int_{-\infty}^{\infty} dl \int_0^{\infty} dE \frac{l^m}{\tau^n} P(E, l, t), \quad (23)$$

to give

$$\partial_t P_{m,n} = \dot{\gamma} m P_{m-1,n} + \frac{\dot{\gamma} n}{x} P_{m+1,n} - P_{m,n+1} + \frac{1}{1+n/x} P_{0,1} \delta_{m,0} \quad (24)$$

for $m, n = 0, 1, 2, \dots$. Listing $P_{m,n}$ in the state vector \mathbf{s} , and noting that $P_{1,0} = \sigma$ (*i.e.* the macroscopic stress is the average of the local ones) we recognise this to fit the framework in the main text with infinite dimensional \mathbf{s} .

As described in Ref. [27, 43], this model is rendered spatially aware by means of a numerical simulation in which we evolve $j = 1 \dots m$ SGR elements on each of $i = 1 \dots n$ streamlines, corresponding to $y = 0 \dots 1$ with periodic boundary conditions. The stress on streamline i is $\sigma_i = (1/m) \sum_j l_{ij}$. At any timestep a waiting time Monte Carlo algorithm chooses stochastically the next element to jump. Supposing the jump occurs at element ij when its local strain is $l = \ell$, force balance is then imposed by updating all elements on the same streamline as $l \rightarrow l + \ell/m$. Diffusive coupling of the dynamics on neighbouring streamlines is included by further adjusting the strain of three randomly chosen elements on each adjacent streamline $i \pm 1$ by $\ell w(-1, +2, -1)$.
